Study Regarding the Influence of the Biasing Network in Designing a Switchable Frequency Selective Surface

Study Regarding the Influence of a Control Network in Designing a Switchable Frequency Selective Surface

Andrei-Marius Silaghi
Dept. of Measurements and Optical Electronics
University Politehnica Timisoara
Timisoara, Romania
andrei.silaghi@upt.ro

Farzad Mir
Dept.t of Electrical and Computer Engineering
University of Houston
Texas, USA
farzadmir1992@gmail.com

Aldo De Sabata
Dept. of Measurements and Optical Electronics
University Politehnica Timisoara
Timisoara, Romania
aldo.de-sabata@upt.ro

Ladislau Matekovits
Dept. of Electronics and Telecommunications
Politecnico di Torino
Torino, Italy
ladislau.matekovits@polito.it

***Abstract*—In this paper it is suggested how to design a switchable Frequency Selective Surface. The simulations of the two distinct metallic constructions are performed, initially with no control network present and afterwards with the same topology control network (having the function to bias the active components inside the unit cells). The suggested designs have been evaluated using electromagnetic simulation. Different filtering bands are obtained below 12 GHz using the periodicity of the square-shaped unit cell with an 18 mm edge length.**

***Keywords—component, formatting, style, styling, insert** (key words)*

I. Introduction

The polarization conversion of incident linearly polarized waves into circularly polarized ones, which are less susceptible to distortions, is a function of frequency selective surfaces (FSSs), which are 2D periodic structures [1], [2]. Making these structures adaptable is a natural development of them [3], [4].

The main problem with standard FSS structures is that their reflection and transmission characteristics are dependent on the angle of incidence of electromagnetic waves. Engineers are increasingly introducing lumped elements into designs as remedies for this issue and to create tunable/switchable FSSs, utilizing one of two major variants: using PIN or varactor diodes [5-7]. Furthermore, in designs containing active components, a DC bias network (Control network-CN) must be used. Given the enormous number of research organizations working on it globally, creating tunable/switchable FSSs devices, is one of the most difficult topics in many scientific domains [2–8].

Several tunable/switchable structures have been proposed by some of authors in the past in [2], [5]. Firstly, circular and elliptical designs have been tackled, with the objective of obtaining notch filtering and polarization filtering [5] and in terms of CN, two crossed microstrip lines are utilized. Then rectangular designs are proposed [2] for multiple bands filtering. In this case, the main FSS structure was connected to three parallel CN microstrip lines by via holes [2].

Another topic is regarding phase and amplitude control which was tackled in the recent literature [4], [6]. For example, in [4] with the purpose of Lidar applications a plasmonic pixel is introduced with voltage biasing of the component antenna involved. Then in [6] the authors propose a tunable metasurface which achieved the arbitrary phase and amplitude tuning while preserving a comparatively low physical profile by combining separate phase and amplitude control modules under the guidance of analogous circuit models.

This article is organized as follows. The proposed solutions without CN are discussed in Section 2, after which the operation is assessed using an electromagnetic simulation. an electromagnetic simulation is used to evaluate the operation. This section also addresses parametric variations to illustrate the switchability of the structures. Section 3 reports the results with the CN being present. To add more depth to the investigation, field images for the structures and CN lines are created and explained. The last section includes conclusions.

II. Initial Structures

In this section we cover the structures without the control network (CN) being present. Firstly, the concept of a main structure and a cut-slot structure is provided, both having a symmetric unit-cell. The configurations of the unit-cell (top view) shown in Fig. 1(a)-main and 1(b)-cut-slot include metallic rectangular form loadings constructed on FR4 substrate layer, with ε_r=4.3$ and tan σ=0.025. Grey color is used to represent the metallic areas. Following is an explanation of how the two graphs, each with eight cut-slots, differ from one another.

Both of the structures have a thickness of h_1=1.58 mm. The smaller rectangle's sides are D_a=8 mm and D_b=6 mm whilst the bigger rectangle's sides are D_u=14 mm and D_v=12 mm. The two aforementioned rectangles are linked together by two cross lines that are the same width, W=1 mm, and have lengths of 12 mm (L_h) and 14 mm (L_v), respectively, for the horizontal and vertical microstrip lines. The horizontal lines are 0.35 mm wide, while the outside vertical lines are 1 mm wide, the same as the two crosslines.

In the present study, a pair of four PIN diodes operating in the 100 MHz–30 GHz frequency band are proposed to be used

for tuning the proposed FSS. Diodes in the structure necessitate thinking about substrate placement. Consequently, as shown in Fig. 1(b), cut-slots are prepared. The length and width of the cut-slots are L_{cut}=1 mm and W_{cut}=0.47 mm, based on the size of the diodes.

The PIN diode, whose operation is governed by the biasing voltage given to the structure, also governs the operation of the FSS. When the CN is connected to high voltage, the PIN diode behaves in a manner that is consistent with a small R (ON-state), which indicates a nearly short-circuit. On the other hand, PIN diodes behave like capacitors (OFF-state) when the structure is supplied with little power [mir, 2021]. The structure becomes tunable in relation to the voltage drop at the generator terminals because the diodes either create a short-circuit or a capacitive load, which modifies the resonant frequency.

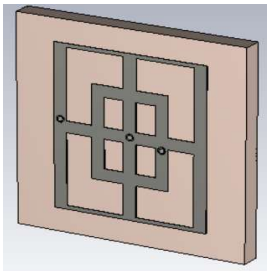

Fig. 1.(a) Main structure unit cell.

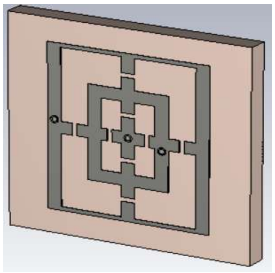

Fig.1.(b) Cut-slot structure unit cell.

Results from the simulation package [CST] for both TE and TM-incidence for the main structures stated geometry are shown in Fig. 2. Theta = 0 and phi = 0 (the angles of spherical coordinates with respect to the reference frame in Fig. 1) are for normal incidence.

So, in Fig. 2, for the main structure, we can observe the next stopbands: for TE mode we can notice a first notch centered at 8.66 GHz, with a -10dB stopband between 6.54 GHz and 9.98 GHz, and also a second smaller one centered at 11.35 GHz (between 11.17 - 11.67 GHz). Next, in TM case the center of the stopband is at 7.82 GHz, and it spans between 6.5 GHz and 8.79 GHz.

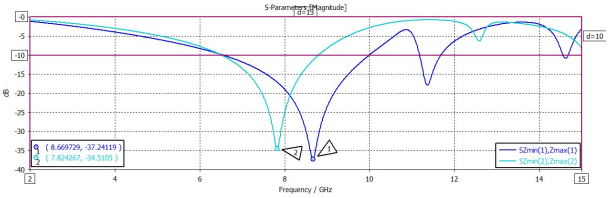

Fig. 2. Main structure results - without CN (TE and TM modes).

Afterwards, in Fig. 3 the cut-slot structure simulation result is presented. Starting with TE mode, this time three -10 dB stopbands appear: the first between 4.19 GHz and 4.96 GHz (the notch being centered at 4.66 GHz) and the second between 8.85 GHz – 10.64 GHz (E) with a notch at 9.94 GHz. The third one, being the smallest, is between 11.64 GHz - 12.04 GHz. If we discuss about the TM mode, it is also visible in Fig. 3, displaying two stopbands: one between 3.70 GHz and 4.21 GHz (with a notch at 3.98 GHz) and another between 9.48 GHz and 10. 49 GHz, this time the notch being centered at 10.07 GHz.

After that, parametric analyses of the variation of transmittance with angle theta for both the main structure and the cut-slot structure were conducted. First, a parametric study in TE incidence was conducted for the main structure. The theta angle was adjusted in steps of 15 degrees between 0 and 45 degrees. According to the outcome of Fig. 4, the highest notch is moved to higher frequencies when this parameter is increased. At lower frequencies, a second notch likewise appears. For the TM case (not reported in this paper), a different behavior is observed for the main structure: there is only a slight shift between 7.82 GHz and 7.65 GHz if we vary theta parameter from 0 to 45 degrees.

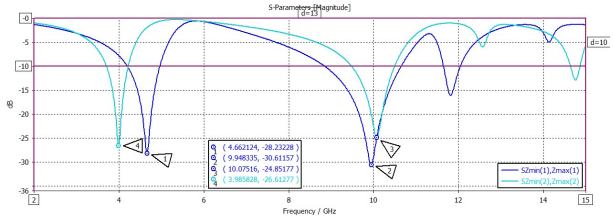

Fig. 3. Cut-slot structure without CN (TE and TM modes).

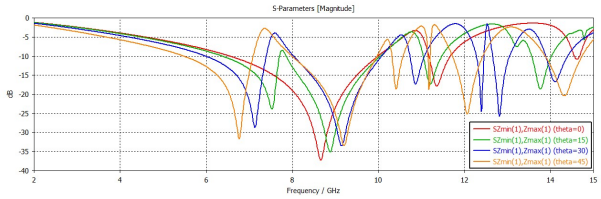

Fig. 4. Parametric study of theta, for the main structure without CN (TE mode).

The results for theta variation, for the cut-slot structure in TE incidence is shown in Fig. 5, where it can be seen that it exhibits a distinct behavior from the main structure. This time, the second stopband slightly widens as theta increases, while the first notch (about 4.66 GHz) essentially stays the same.

Studying the outcome for the cut-slot design in TM incidence (not reported in this spaper), one can distinguish that: once more, as theta changes, the first notch stays the same while the other notches shift to lower frequencies.

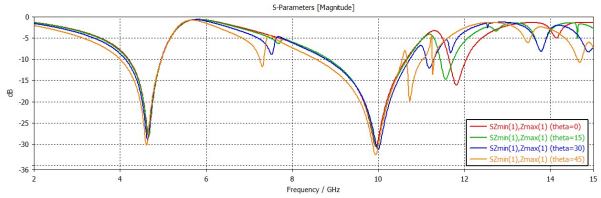

Fig. 5. Parametric study of theta, cut-slot structure without CN (TE mode).

III. Structures with Control Network

Next, we cover the structure with the CN being present. In this section, three parallel CN microstrip lines are connected to the main FSS structure via holes structures (one via hole connects one CN line). In relation to the edge of the PCB with the pattern, these lines are situated on the opposite side. Microstrip lines inserted on the ground side of the construction have the following parameters: L_m = 18 mm, W_m = 0.4 mm, and a 0.6 mm gap separates neighboring microstrip lines.

Each individual microstrip line is biased by a constant potential throughout operation, resulting in an externally adjustable voltage drop among each of them. The varactors are

dynamically biased using these two values. The lines for the various columns of the FSS are linked together in the current design at one of the PCB's borders (details are shown below).

Additionally, via-holes are inserted to link the feeding lines to the main structure. Following are the via-hole locations as measured in *x* direction from the unit cell's edge: the central via-hole is located at 9 mm from the edge (D2 in Fig. 6), whereas the left via-hole is at 3.5 mm (D1 in Fig. 6) and the right via-hole is at 6.5 mm (D3 in Fig. 6).

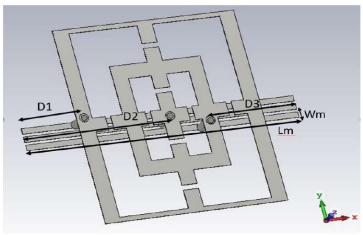

Fig. 6. Location of CN and via holes.

Furthermore, in Fig. 7, for the main structure, we can observe the simulation results with the CN being present. For TE mode we can notice that the principal notch is again centered at 8.66 GHz, with a -10dB stopband between 6.57 GHz and 9.88 GHz (slightly different than the one without the CN), but this time also a very small third notch appears centered at 10.3 GHz. Bigger differences appear in TM mode (Fig. 7): in comparison with Fig. 2, in this case several stop bands appear.

Next, in Fig. 8 we can see the cut-slot structure simulation results in TM and TM modes, with CN incorporated. Firstly, in TE mode again two stopbands appear, centered at 4.68 GHz and 9.82 GHz, whilst in Fig. 3 we noticed these stopbands at 4.66 GHz and 9.94 GHz respectively. The CN has again greater influence in TM mode: three different stopbands appear in Fig. 8 in comparison with Fig. 3.

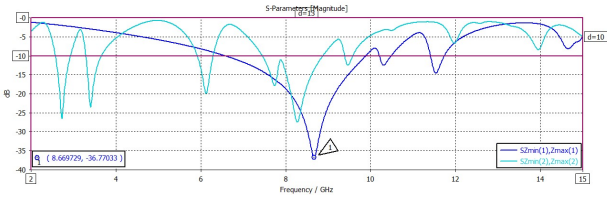

Fig. 7. Main structure with CN (TE and TM modes).

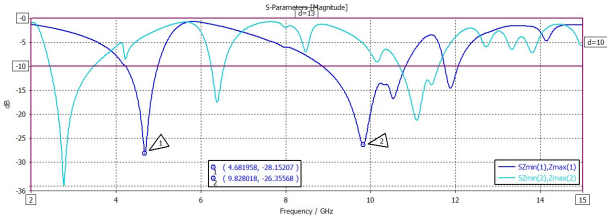

Fig. 8. Cut-slot structure with CN (TE and TM modes).

Next, field images of surface current density are presented for each of the main and cut-slot structures in order to further clarify the aforementioned results with the presence of the CN.

The main structure is addressed first. The frequency chosen for the calculation of field images is 8.66 GHz because our resonance is centered at this frequency (Fig. 9). The maximum magnetic field, shown in Fig. 9, is 114 A/m for an excitation of 1 V/m. Additionally, the exterior of the design exhibits the largest surface currents; as a result, the large rectangles dimensions (D_u and D_v) serve as the resonances source. Since there is a minimal current flowing in the orthogonal direction (*x* in this instance), there is low cross-pol coupling as well.

The field pictures are then plotted at 4.68 GHz and 9.82 GHz since these frequencies correspond to the resonances of the cut-slot structure. Comparable to the inheritance from the main structure, the initial resonance (4.68 GHz) also inherited the large rectangular dimensions. High levels of the magnetic field (263 A/m) from Fig. 10 serve as examples of this. Once more, the value of the current flowing in the *x* direction is very small (Fig. 10).

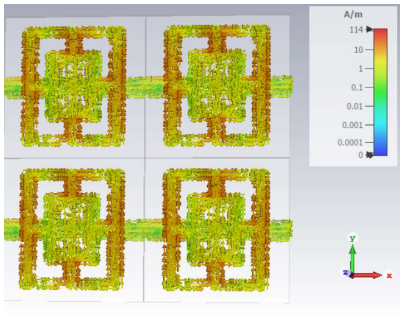

Fig. 9. Field images of surface current density, main structure with CN present, at 8.66 GHz.

The short interior rectangle dimensions (D_a and D_b) of the design are the cause for the appearance of the second resonance (9.82 GHz). In this instance, the current going in the *x* direction is strong whereas the one flowing in the *y* direction is extremely weak (Fig. 11). The surface current density images at 9.82 GHz, where the lowest values are observed at the exterior part of the structure (Fig. 11), further strengthen this assertion.

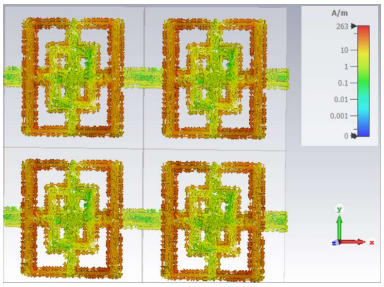

Fig. 10. Field images of surface current density, cut-slot structure with CN present, at 4.68 GHz.

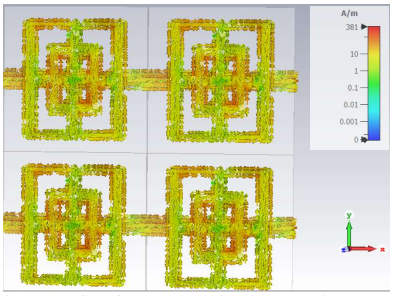

Fig. 11. Field images of surface current density, cut-slot structure with CN present, at 9.82 GHz.

In order to show how the CN lines affected how the resonances appeared, surface currents were also calculated on

the opposite side of the design (Fig. 12 and Fig. 13). Surface currents at 4.68 GHz have very low values on the CN lines side (Fig. 12), but surface currents at 9.82 GHz have substantial values on the CN lines side (Fig. 13). Therefore, it can be said that the CN lines have an effect on how the resonance at 9.82 GHz manifests itself.

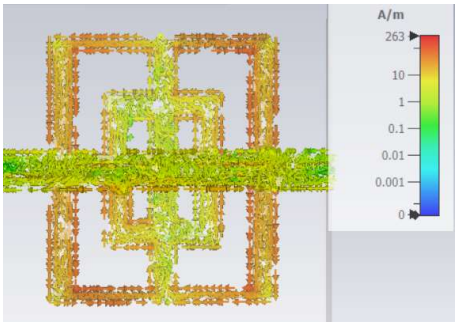

Fig. 12. Field images of surface current density, cut-slot structure with CN present, at 4.68, CN lines GHz.

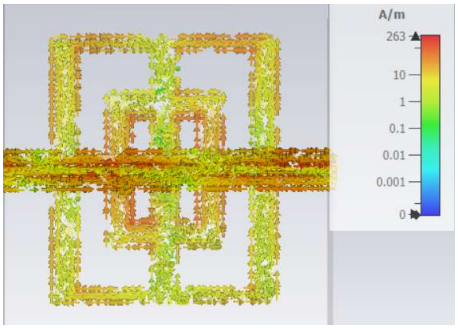

Fig. 13. Field images of surface current density, cut-slot structure with CN present, at 9,82, CN lines GHz.

IV. Conclusions

For frequencies below 12 GHz, a switchable FSS with several configurations that functions as a band-stop spatial filter has been suggested in this study. Filtering is seen in two structures (main and cut-slot) that have first a CN absent, and then a CN integrated.

The switchability of the suggested structures has been proven through a parametric investigation for the colatitude angle (by means of electromagnetic simulation). Finally, field images of surface current density are provided in order to ensure depth to the proposed work.

Acknowledgment

This work was supported by a grant of the Ministry of Research, Innovation and Digitization, CNCS - UEFISCDI, project number PN-III-P1-1.1-PD-2021-0010, within PNCDI III.

References

[1] Munk, B.A. Frequency Selective Sufaces: Theory and Design. In Frequency Selective Surfaces; John Wiley & Sons, Ltd.: Hoboken, NJ, USA, 2000

[2] A.-M. Silaghi, F. Mir, A. De Sabata, L. Matekovits, "Design and Experimental Validation of a Switchable Frequency Selective Surface with Incorporated Control Network", *Sensors* **2023**, *23*,4561. https://doi.org/10.3390/s23094561

[3] Jeong, H.; Le, D.H.; Lim, D.; Phon, R.; Lim, S. Reconfigurable Metasurfaces for Frequency Selective Absorption. Adv. Opt. Mater. 2020, 8, 1902182

[4] Calà Lesina, A.; Goodwill, D.; Bernier, E.; Ramunno, L.; Berini, P. Tunable Plasmonic Metasurfaces for Optical Phased Arrays. IEEE J. Sel. Top. Quantum Electron. 2021, 27, 4700116

[5] F. Mir, L. Matekovits, A. De Sabata, "Symmetry-breaking manipulation in the design of multifunctional tunable frequency selective surface", AEU Int. J. Electron. Commun. 2021, 142, 154003.

[6] Zheng, B.; Ren, H.; An, S.; Tang, H.; Li, H.; Haerinia, M.; Dong, Y.; Fowler, C.; Zhang, H. Tunable Metasurface with Dynamic Amplitude and Phase Control. IEEE Access 2021, 9, 104522–104529

[7] Xing, B.B.; Liu, Z.G.; Lu, W.B.; Chen, H.; Zhang, Q.D. Wideband Microwave Absorber with Dynamically Tunable Absorption Based on Graphene and Random Metasurface. IEEE Antennas Wirel. Propag. Lett. 2019, 18, 2602–2606.

[8] Ebrahimi, A.; Shen, Z.; Withayachumnankul, W.; Al-Sarawi, S.F.; Abbott, D. Varactor-Tunable Second-Order Bandpass FrequencySelective Surface With Embedded Bias Network. IEEE Trans. Antennas Propag. 2016, 64, 1672–1680.